frontiers | Frontiers in Materials

TYPE Original Research
PUBLISHED 15 December 2022
DOI 10.3389/fmats.2022.1037386

OPEN ACCESS

EDITED BY
Yang Zhu,
Zhejiang University, China

REVIEWED BY
Ângela Maria Moraes,
University of Campinas, Brazil
Sônia Maria Malmonge,
Federal University of ABC, Brazil

*CORRESPONDENCE
Wei Jiang,
WeiChiang88@163.com

SPECIALTY SECTION
This article was submitted to Biomaterials and Bio-Inspired Materials, a section of the journal Frontiers in Materials

RECEIVED 05 September 2022
ACCEPTED 17 November 2022
PUBLISHED 15 December 2022

CITATION
Zhang L, Li Y and Jiang W (2022), A novel wound dressing material for full-thickness skin defects composed of a crosslinked acellular swim bladder. *Front. Mater.* 9:1037386. doi: 10.3389/fmats.2022.1037386

A novel wound dressing material for full-thickness skin defects composed of a crosslinked acellular swim bladder

Lifeng Zhang, Yan Li and Wei Jiang*

Department of Orthopedics, The First Affiliated Hospital of Anhui Medical University, Hefei, China

The repair of widely pervasive skin defects remains a daunting challenge. Previous research on skin defects has applied artificial skin, although this is limited by high cost and complex fabrication. Biomaterials have attracted much attention in recent years due to their accessibility and excellent biocompatibility. We designed a novel cell-scaffold material for wound dressing using swim bladders; the mechanical properties of these could be enhanced by EDC/NHS crosslinking. This material possesses many advantages, including adequate porosity, high mechanical strength, and good thermal stability. In particular, swim bladders after EDC/NHS crosslinking have an increased denaturation temperature and higher tensile strength, along with the ability to be harmlessly colonized in the wound sites of rabbit models, followed by rapid vascularization and cell growth with mild inflammatory reactions. The successful implantation of swim bladders proves that this cell scaffold with its unique features can be an outstanding wound dressing material.

KEYWORDS

swimming bladders, EDC/NHS crosslinking, skin repairment, scaffold, wound dressing

Introduction

Due to the lack of dermis, skin areas with large-area defects are not able to repair themselves—a severe challenge in dermatology and orthopedics (You et al., 2019). Traditional *in situ* suturing causes an increase in local skin tension, resulting in surgery failure. As an alternative, tension-free suturing with autologous skin grafts is currently the most widely employed method for the treatment of local skin defects, as well as the most reliable way of restoring skin structural integrity (Birkelbach et al., 2020). However, the limited range of autologous skin still cannot meet clinical needs when the defective skin area is too broad (Fu et al., 2014). Allogeneic skin-graft materials have been studied as another alternative (Łabuś et al., 2022), but they still face several drawbacks, such as immunological rejection and the potential spread of infectious diseases (Qiu et al., 2016). In addition, these materials are always associated with the disadvantage of poor mechanical strength, while high mechanical strength is an essential factor in constructing skin repair materials (Aghamirsalim et al., 2022). There is therefore a pressing need to

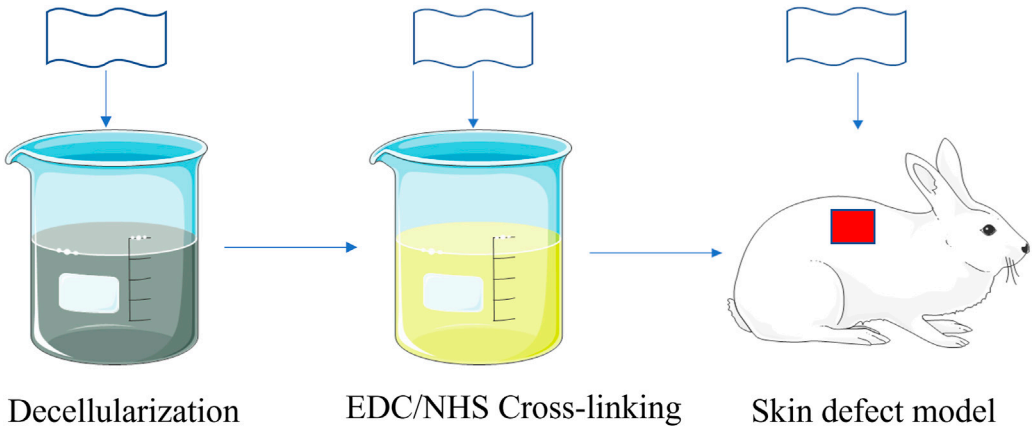

FIGURE 1
Schematic illustration of fabricating and implantation of EDC/NHS Cross-linking swimming bladders.

prepare materials with excellent mechanical properties and biocompatibility comparable with those of human skin.

To address this problem, numerous studies on suitable materials for skin repair have been conducted. Synthetic materials such as chitosan hydrogel (Yoon et al., 2017; Behr and Ganesan, 2022), crosslinked poly (N-vinylpyrrolidone) (PVP) hydrogel membranes (Thongsuksaengcharoen et al., 2020), and polyethylene glycol (PEG) hydrogel membranes have been reported to induce an appropriate response of skin reconstruction in a limited area (Chatterjee et al., 2019). However, synthetic materials are always associated with unsatisfying issues of poor biocompatibility, non-degradability, high cost, and complex fabrication methods, making it impossible to achieve mass production (Li et al., 2015). Natural collagen material plays a vital role in promoting wound healing since it is an essential substance that exists abundantly in human tissues (Wang et al., 2019; Jafari et al., 2020). These materials are usually combined with other materials to enhance mechanical strength (Attasgah et al., 2022; Liu et al., 2022). Collagen-rich animal extracellular matrix (ECM) is of great interest because collagen is a chemical attractant of fibroblasts. Combined with a porous structure, it can also promote angiogenesis and fibroblast growth (Gentile and Garcovich, 2021; Saini et al., 2021). In addition, it has been found that ECM has certain antibacterial properties (Meng et al., 2021), which might be related to rapid vascularization at the repair site to remove bacteria. Traditionally, the acquisition of matrix materials derives from the Achilles tendon and pericardium of mammalian animals (Chen et al., 2021), but potential infection and religious barriers are still a big barrier to this. In recent years, several studies have focused on the collagen of marine animals (Li et al., 2017; Mredha et al., 2017), among which collagen from swim bladders has attracted considerable interest for its low cost and accessibility (Fernandes et al., 2008; Mredha et al., 2015; Gaurav Kumar et al., 2017). Previous studies have demonstrated that the tissue of swim bladders is mainly composed of collagen fibers (more than 80%) and some fibroblasts (Eun et al., 1994). Its unique triple helix structure makes it more thermally stable than other collagen sources, and adequate porosity also makes it an ideal choice (Rittié, 2016). Furthermore, there are no reports about zoonosis of swim bladders, confirming them as a reliable and promising wound dressing material.

In this study, we constructed a cell scaffold by using swim bladders, and improved their physical and chemical properties by EDC/NHS crosslinking. As a result, the mechanical strength and the protein denaturation temperature can meet the demand for transplantation. Through various characterizations, we can attain tensile strength, elongation at break, porosity, and protein denaturation temperature before and after crosslinking. Additionally, we established a full-thickness skin defect model in rabbits and implanted un-crosslinked and crosslinked swim bladders into the wound sites (Figure 1) to verify whether they can be harmlessly transplanted into mammals. Our study demonstrates that swim bladders with their unique features could be a promising wound dressing material.

Materials and methods

Materials

Phosphate-buffered saline (PBS) solution was obtained by combining sodium chloride, sodium dihydrogen phosphate, and disodium phosphate. 2-(2-[4-(1,1,3,3-Tetramethylbutyl) phenoxy]ethoxy)ethanol (Triton X-100), 3-(3-dimethylaminopropyl)-1-ethylcarbodiimide hydrochloride (EDC), N-hydroxy succinimide (NHS), and sodium 2-

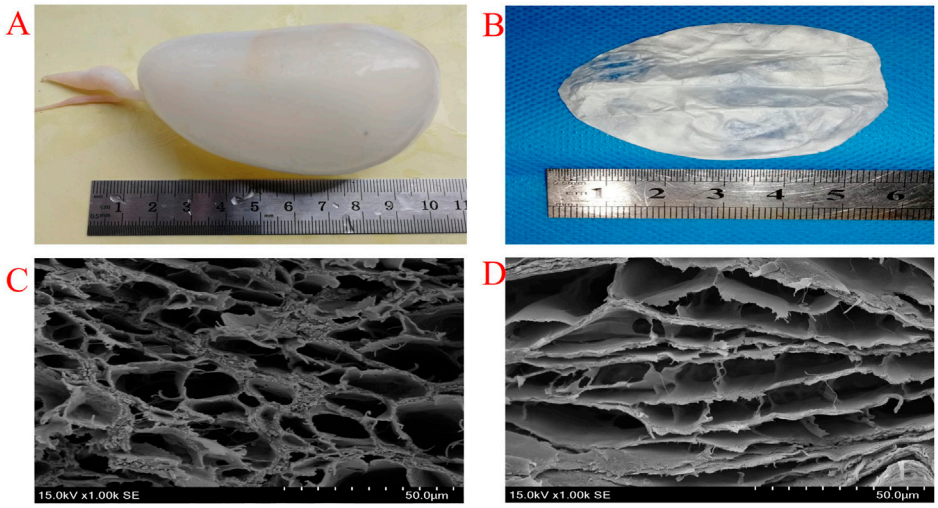

FIGURE 2
Photograph of fresh swimming bladders **(A)** EDC/NHS Cross-linking swimming bladders **(B)** SEM images of uncross-linked **(C)** and EDC/NHS cross-linked **(D)** swimming bladders.

morpholinoethanesulfonate (MES-NA) were purchased from J&K Scientific Ltd.

Sample preparation

Fresh swim bladders of silver carp fish were used in this study (Figure 2A). After removing their outer fat and blood capillaries, the swim bladders were incubated in a PBS (pH 7.4) solution; physiological saline was then used to remove the outer fibers that were loosely attached. Each acellular swim bladder (8 cm * 8 cm) was obtained by treatment with 100 ml 1% Triton X-100 in PBS solution at room temperature (25°C) for 24 h.

EDC/NHS crosslinking

A 50 mmol/L MES buffer solution (pH 5.5) was prepared as follows. First, a drop of concentrated hydrochloric acid was added to 50 ml of distilled water to prepare Liquid A, and then 50 mmol MES-NA was dissolved into 200 ml distilled water to prepare Liquid B. Liquid A was gradually added dropwise to Liquid B under constant stirring until the pH was 5.5 to prepare the MES buffer solution. The EDC/NHS crosslinking solution with a molar ratio of EDC to NHS of 4: 1 (20 mmol·L^{-1}:5 mmol·L^{-1}) was obtained using this solution. Each acellular swim bladder (8 cm * 8 cm) was immersed in the prepared 100 ml crosslinking solution and incubated in the dark at room temperature (25°C) for 12 h. All samples were lyophilized in a freeze drier at −80°C for 24 h (Figure 2B).

Characterization

Surface structure studies using FTIR spectroscopy

The FTIR spectra of all the lyophilized swim bladders (both crosslinked and un-crosslinked samples) were recorded with a Thermo Scientific Nicolet iS50 FTIR in attenuated total reflection mode at room temperature. An IR spectral range of 400–4,000 cm^{-1} was analyzed.

Microstructural evaluation

Scanning electron microscopy (SEM) was used to observe the microstructure morphology of the dehydrated 0.8 × 0.8 cm samples. The samples were coated with a thin layer of gold for 120 s at a 15 mA discharge current. After coating, the pore-size distribution of the samples was acquired at a voltage of 15 kV (Nova Nano SEM 450 FEI Company USA).

Material stability

To evaluate thermodynamic stability, universal differential scanning calorimetry (DSC) was performed by calorimetric heat flow (mW mg^{-1}) with temperature (°C) growth. Briefly, approximately 5 mg samples (n = 3) from both groups were sealed in a DSC pan and heated from 0 to

100°C at an increase rate of 10°C min^{-1} in a N_2 gas environment (Q2000 TA USA).

Mechanical performance

We completely immersed the samples in physiological saline for 10 min. The samples were cut into 3.0 *0.8 cm sections in the fiber bundle direction. The tensile properties of crosslinked and un-crosslinked samples (n = 4 for each group) were pulled at a rate of 100 mm min^{-1}using a tensile machine at room temperature (Instron, USA).

Mammalian models

We conducted the study on 24 healthy white male rabbits weighing between 2 and 2.5 kg. All 24 rabbits were under intravenous anesthesia using 1.5% pentobarbital (2 ml/kg). After routine disinfection of the skin, a 3*3 cm^2 skin full-thickness incision was made on the dorsum of all rabbits with a scalpel. The rabbits were divided randomly into three groups. Group A involved rabbits without any treatment except for the dressing fixed to the wound. In Group B, the defect of rabbits was repaired with un-crosslinked acellular swim bladders by means of absorbable suture. In Group C, the incisions of the rabbits were repaired with EDC/NHS-crosslinked acellular swim bladders by an absorbable suture. After the operation, each group of rabbits was reared separately.

This research was approved by the Ethics Committee of Anhui Medical University (LLSC20221117).

General observation

We conducted daily gross observation of wound repairs in the rabbits from all three groups. A camera was used to record general photos of repair in each group for 7 , 14 , 21 , and 28 days to determine whether the wounds were ulcerated and whether there was purulent exudate. The wound area of each group (Sw) and the original incision area (So) were obtained utilizing ImageJ software. The wound healing efficiency (η) was calculated as follows:

$$\eta = \left[\frac{S_o - S_w}{S_o}\right].$$

Histological observation

Two rabbits from each group were sacrificed on the 7th, 14th, 21st, and 28th days after surgery. The wound sites, together with the tissues adjacent to the normal skin, of all the rabbits were collected and fully fixed with 4% paraformaldehyde before hematoxylin-eosin (H&E) staining and Masson's staining. The angiogenesis, fibroblast distribution, growth of inflammatory cells, and epithelialization of the repair sites of all rabbits were observed after H&E staining, while the arrangement of collagen fibers was observed after Masson's staining through a light microscope. The histological scoring system described by Kumar et al. (2015) was used.

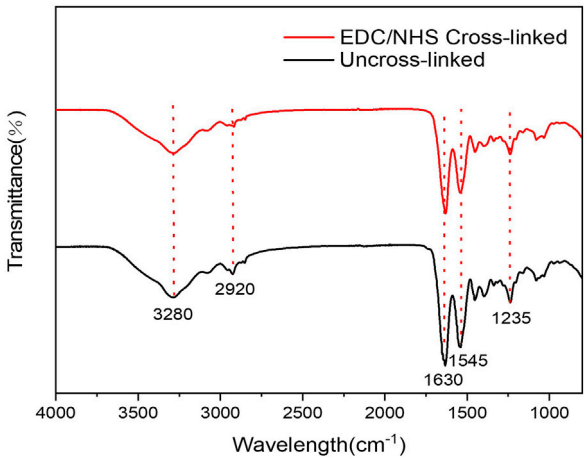

FIGURE 3
ATR-FTIR spectra of swimming bladders before and after cross-linking.

Statistical analysis

All measurements are presented as the means ± standard deviations (SDs). Differences between groups were analyzed with LSD-t-tests with SPSS software, version 23.0 (IBM, Armonk, NY, USA). Differences with p-values of <0.05 were considered significant.

Results

Fabrication of EDC/NHS crosslinked acellular swim bladders

The purpose of decellularization is to reduce the antigenicity of swim bladders, which can cause inflammatory reactions. A significant advantage of EDC/NHS solution as the crosslinker in this study is that it only promotes the reactions between carboxyl groups and amino groups from collagen molecules without leaving any harmful group in the system. The crosslinking process does not influence the structure of swim bladders, as shown by FTIR spectroscopy (Figure 3). The peak at 3280 cm^{-1} refers to the stretching vibration of N-H from the protein peptide bonds:

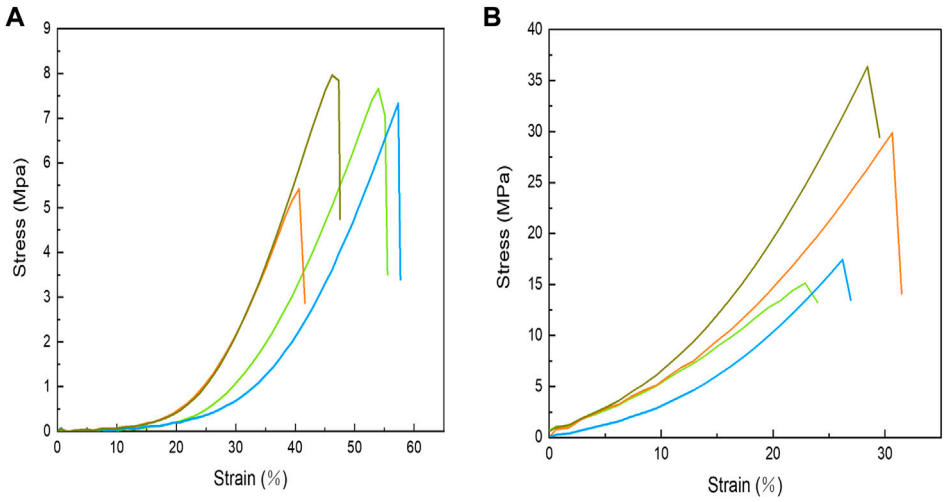

FIGURE 4
Stress-strain curves of uncross-linked **(A)** and EDC/NHS cross-linked **(B)** swimming bladders.

the peak at 2920 cm^{-1} is for the asymmetric stretching vibration of CH_2, the peak at 1630 cm^{-1} represents the stretching vibration of C=O, the peak at 1545 cm^{-1} is for the bending vibration peak of N-H and C-N, and the peak at 1235 cm^{-1} represents the CH_2 vibration of the glycine and proline residues from the peptide chains. No new characteristic peaks were detected, and the typical peak did not shift after EDC/NHS crosslinking, demonstrating that swim bladders maintain their pristine structure after crosslinking. The FTIR results indicate that the evolution of collagen molecules after crosslinking is mainly caused by the increase in the number of hydrogen bonds originating from new C=O and N-H bonds in amide bonds after covalent crosslinking.

Pore structure and stability

High porosity structures are observed in the fracture sections of both un-crosslinked and crosslinked swim bladders (Figure 2C, Figure 2D). The pore diameter is approximately 25.35 ± 5.18 μm in un-crosslinked swim bladders and approximately 21.12 ± 4.94 μm in crosslinked swim bladders. Although pore size is reduced after crosslinking, it is still the ideal size for cell proliferation. The reduction in pore size is mainly because collagen molecules condense during crosslinking. The denaturation temperature of the swim bladders after EDC/NHS crosslinking is 74.6°C, which is higher than that of the un-crosslinked swim bladders (Supplementary Figure S1). This result indicates that crosslinking can increase the denaturation temperature of swim bladders, in which collagen molecules are allowed to form a network to create a denser structure. In particular, the denaturation temperature of both crosslinked and un-crosslinked swim bladders meets the demand for survival in the human body.

Mechanical properties

Uniaxial tensile tests were conducted to examine the mechanical properties of swim bladders to ensure that they have the proper mechanical strength to cover the wound sites (Figure 4). Obviously, the tensile strength of un-crosslinked swim bladders (7.09 ± 1.14 MPa) is lower than that of EDC/NHS crosslinked swim bladders (24.71 ± 10.11 MPa), while the results are opposite in terms of the elongation at break. The strengthening mechanism can be mainly attributed to the collagen molecules condensing during crosslinking, which provides a more rigid structure in EDC/NHS crosslinked swim bladders.

Skin regeneration in mammalian models

No animal died during the entire experiment, and observation of wound repair revealed no acute suppurative inflammation (Figure 5). On the 7th day, wounds were covered with a soft and fragile pale-brown mass having a mildly desiccated top surface in Group A. The grafts of Groups B and C became light brown and dry, and the size of the wounds did not significantly differ from that of Group A. On the 14th day, the wound site of Group A formed a distinct thick skin tissue and was elliptical in shape, while there was no

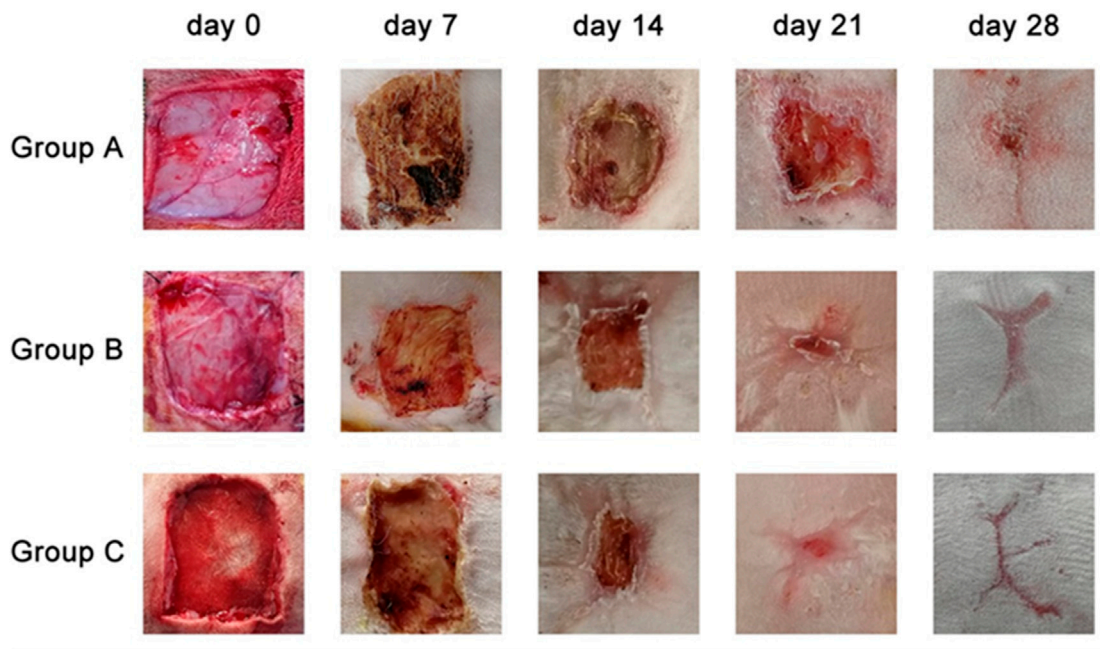

FIGURE 5
General views of the wound sites from three different groups on 7th day, 14th day, 21st day, 28th day.

TABLE 1 Mean ± SE of total wound area (mm^2) of skin wounds in rabbits of Groups A, B, and C at Days 0, 7, 14, 21, and 28.

	0	Day 7	Day 14	Day 21	Day 28
Group A	905.80 ± 1.31	756 ± 14.19	455.8 ± 19.72	320.51 ± 11.71	9.50 ± 12.22
Group B	907.12 ± 1.08	712.8 ± 4.14	329.54 ± 15.79	102.82 ± 12.80	Healed
Group C	907.10 ± 1.28	706.5 ± 3.66	239.01 ± 12.03	37.75 ± 6.30	Healed

significant change in the graft color in Groups B and C compared to the 7th day, except for a reduction in wound size. On the 21st day, the top brown layer further dried and detached, and newly formed epidermis covered the whole surface of the wounds. The brown upper layers of Groups B and C were further dried and detached, while the inner layers of the grafts were perfectly combined with the wounds, and the wound sites were covered by the newly formed epidermis. On the 28th day, there were still small wounds in Group A that did not completely heal, while the wounds in Groups B and C were completely repaired.

Throughout the whole healing process, the average wound area of Groups B and C on the 7th, 14th, and 21st postoperative days decreased significantly ($p < 0.05$) compared with Group A. On the 28th day, the wounds that were completely repaired in Groups B and C remained in Group A. Furthermore, Group C had a higher repair efficiency and repair rate than Group B (Table 1).

Histopathological analysis

Histological experiments were conducted in rabbits from all groups (Figures 6 and 7, Table 2). On the 7th day, Group A had no significant epitaxial growth but many inflammatory cells. Furthermore, moderate fibrous tissue hyperplasia and scarcely any process of neovascularization could be observed in the extracellular matrix in Group A. The total histopathology score was 20. In Group B, the histological changes were similar to those in Group A except for mild epithelialization and fibrous tissue formation; more inflammatory cells at the wound sites could also be detected. The total histopathology score was 17. Epithelialization, moderate inflammation, and mild fibrous tissue hyperplasia could be seen in Group C. A minor number of collagen fibers were well aligned, with a total histopathology score of 15.

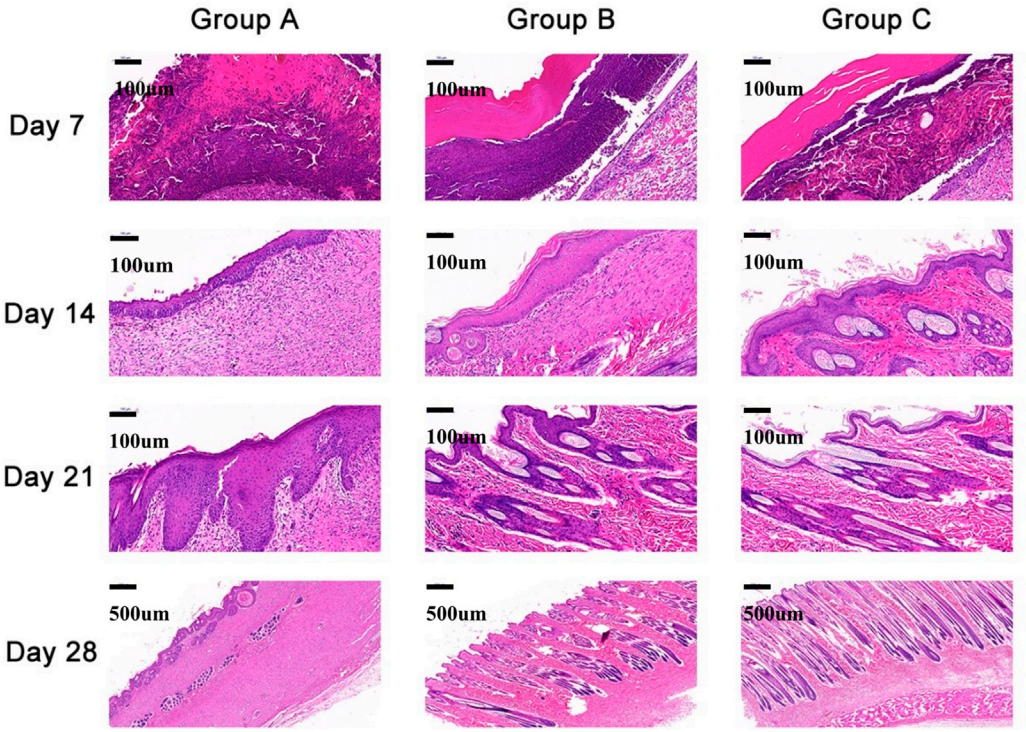

FIGURE 6
Representative images of H&E-stained histologic wound sections of group **(A–C)**.

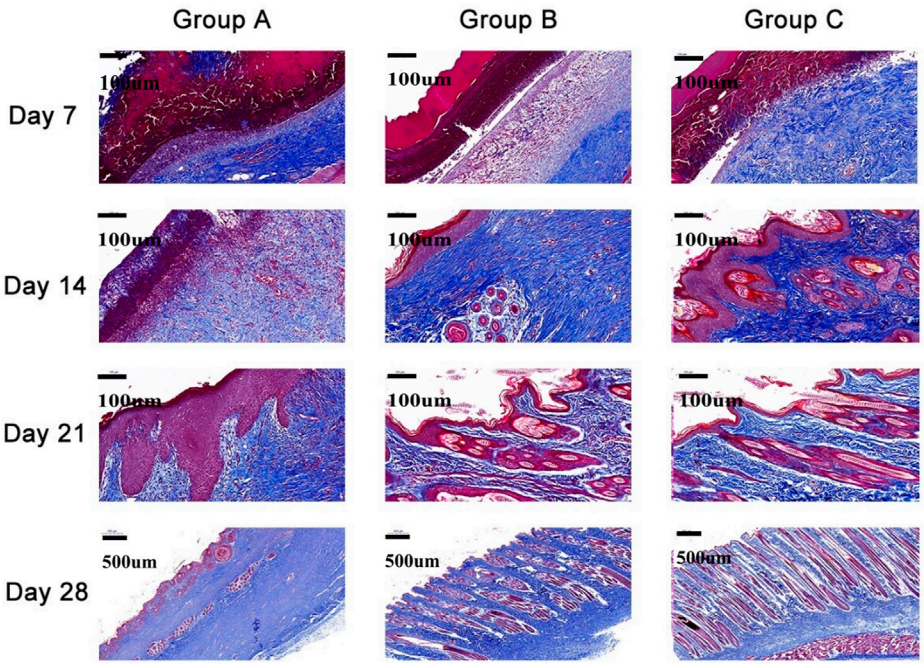

FIGURE 7
Representative images of Masson histologic wound sections of group **(A–C)**.

TABLE 2 Histological scores of wounded tissues in Groups A, B, and C at Days 7, 14, 21, and 28.

	Time interval											
	Day 7			Day 14			Day 21			Day 28		
	A	B	C	A	B	C	A	B	C	A	B	C
Epithelization	3	2	2	2	2	2	1	1	1	1	1	1
Inflammation	4	3	2	2	2	1	1	1	1	1	1	1
Fibroplasia	3	2	2	3	2	2	2	1	1	1	1	1
Collagen density	3	3	2	3	2	2	2	1	1	1	1	1
Collagen arrangement	3	3	3	3	2	2	2	2	2	2	1	1
Glandular	4	4	4	4	3	3	3	2	2	2	1	1
Total	20	17	15	17	13	12	11	8	8	9	7	7

On the 14th day, partial epithelial formation, moderate fibrous tissue hyperplasia, and mild inflammation of the dermis were observed in Group A. Collagen fibers were thinner and less dense, with a histological score of 17. In Group B, the dermis had mild fibrous tissue hyperplasia and a small amount of glandular hyperplasia, and the collagen fibers were denser, thicker, and well arranged, with a histopathology score of 13 at this stage. In Group C, apart from the increased order of collagen fibers, the histological changes were almost the same as those of Group B, and the histopathological score was 12.

On the 21st day, all groups completed epithelialization, and inflammation gradually subsided during the healing process. The collagen fibers in Group A were denser than before, with a small amount of glandular hyperplasia, with a histopathology score of 11. In Groups B and C, mild neovascularization, a moderate number of glands, and hair follicles and other skin appendages were generated, with a histological score of 8.

On the 28th day, the hair follicles, collagen arrangement, glands, and other skin appendages in Group A were less than those in normal skin, while the rest were similar to normal skin. The histology score was 9. In Groups B and C, healing was completed. Epithelialization, collagen arrangement, and dermal appendage formation are almost indistinguishable from those in normal skin. The histological score was 7.

Discussion

Skin wound healing is an extremely complex and dynamic process which traditionally includes a series of phases: hemostasis, inflammation, proliferation, and remodeling (Yang et al., 2019). Full-thickness skin wounds can heal naturally but usually take a long time and result in scar formation, which causes skin dysfunction (Shakya et al., 2016). The extracellular matrix scaffolds prepared by removing the cellular components from native tissue are currently used for wound healing and tissue regeneration. Their role is not only of mechanical support to maintain the shape and integrity of tissues but also in cell migration and differentiation during regeneration (Parisi et al., 2021). In the present study, a collagen-rich acellular swim bladder matrix (ASBM) from silver carp fish was prepared using Triton X-100 and crosslinked with EDC. A cell-free porous collagen scaffold remained after chemical decellularization of the fish swim bladder. Proper chemical crosslinking can reduce the immunogenicity of the matrix and enhance mechanical properties (Litowczenko et al., 2021). The wound healing potential of ASBM and ASBM-EDC was compared in full-thickness skin wounds in this study. Planimetry, wound contracture, and histological observations were carried out to evaluate the healing process.

Since biological materials begin to degrade after removal from living organisms and are derived from different species, the material is not suitable for preservation and direct application, so some pretreatment methods are needed to solve these problems. The purpose of pretreatment is to reduce antigenicity, improve the resistance to enzymatic degradation, and maintain good mechanical properties and tissue structure for a longer period of time before transplanting the biological material (Peng et al., 2019). These treatments include chemical methods of crosslinking using glutaraldehyde, polyepoxy compounds, carbodiimides, and genipin. Physical methods such as photooxidation are also used for crosslinking. Unlike other crosslinkers, EDC-mediated crosslinking is “zero-length crosslinking”; that is, it does not constitute a component in the crosslinking itself but directly mediates the formation of amide bonds between carboxyl and amino groups, and there is almost no EDC component in the crosslinked biological material, whose toxicity is far lower than glutaraldehyde and other commonly used chemical crosslinking agents (Priyadarshani et al., 2016). Previous studies have shown that the growth of endothelial cells grown and cultured on EDC crosslinked biomaterials was significantly better than that of endothelial

cells cultured on glutaraldehyde (GA) crosslinked biomaterials (Jayakrishnan and Jameela, 1996). Our data provide evidence that the crosslinked swim bladder tissue has better physical properties than the un-crosslinked. Cell ingrowth into the *in vivo* implantations was also dramatically higher in the crosslinked swim bladder than in the un-crosslinked swim bladder because of better biocompatibility.

Immune rejection after the use of materials to repair full-thickness skin defects is the most important cause of surgical failure (Henderson et al., 2009). Denaturation of collagen leading to the exposure of antigen-determining clusters may additionally be responsible for rendering it immunogenic; denatured collagen can cause an extreme host immune response. After swim bladder collagen is treated with decellularized reagent, the bonds between the protein molecules break and modify from tertiary and secondary structures to more stable primary structures. Therefore, due to the presence of shorter peptide fragments, cell-free collagen materials have a stronger ability to trigger cell-mediated immune (CMI) responses in the host, which can be presented to the immune system and stimulate CD4 lymphocytes through the MHC class II pathway. The crosslinked material has few immunogenic fragments because, when treating the material with different crosslinkers, the site where the bioenzyme acts *in vivo* is masked and the crosslinked material no longer decomposes into smaller peptide fragments to trigger the host immune response (Pati et al., 2012). The results of animal experiments showed that the total IgG response in rabbit serum of the EDC group was significantly reduced compared to that of the no crosslinking group ($p < 0.05$); the ELISA experiment also confirmed this conclusion (Kumar et al., 2015). Similarly, a reduced total IgG responses was also observed in rabbit serum implanted subcutaneously with glutaraldehyde crosslinked bovine pericardium, compared with un-crosslinked bovine pericardial tissue (Singh et al., 2014). No adverse immune reactions were observed in rabbits during the period of this study. This animal experiment provides evidence that, as a skin repair material, crosslinked collagen has lower immunogenicity during skin repair than un-crosslinked collagen.

Gross observation of the defect site is the most reliable parameter for assessing wound healing. Because of the lack of vascularization and water loss, both the ASBM- and ASBM-EDC-implanted matrix colors changed from white to yellow or brown during wound healing and finally fell off as a dry scab on the top layer. The purple morph of the top layers better protects the layer underneath from desiccation. In addition, the formation of the top scab can also make the lower collagen gradually disintegrate and merge with the new collagen of the wound, thus achieving the purpose of repairing the defect. This bilayer membrane, made of a dermal and epidermal portion, is populated in place on the wound bed by its own fibroblasts and epidermal cells, producing a permanent skin replacement with an anatomically functioning dermis and epidermis. This is similar to a previous study, where 1-ethyl-3-(3-dimethylaminopropyl) carbodiimide hydrochloride (EDC) crosslinked acellular small intestinal submucosa matrix was used to repair full-thickness skin wounds in rabbits and underwent similar gross structural changes (Kumar et al., 2015). In our study, similar results were observed in both matrices with regard to wound contraction. As healing progressed, significantly ($p < 0.05$) less contraction was observed in wounds with implants compared to Group A. Acellular matrix may stimulate neoangiogenesis, leading to faster skin regeneration. This view was confirmed by histological observations. In this study, implantation of ASBM and ASBM-EDC on full-thickness skin wounds in rabbits provided better epithelization and improved blood vessel supply and collagenization on all post-implantation days compared with Group A. The crosslinked acellular swim bladder matrix from silver carp fish promoted biological activities that resulted in faster healing of full-thickness skin wounds in rabbits. In this study, EDC-crosslinked ASBM provided a significant decrease in the severity of the inflammatory response. This activity might be related to the antigen masking activity of the EDC on lymphocyte proliferation.

Furthermore, swim bladder-derived materials have two other advantages. First, they could alleviate patient anxiety after receiving tissue from traditional bovine- or porcine-derived pericardium or calcaneus tendons due to the outbursts of some zoonoses, such as foot-and-mouth disease and bovine spongiform encephalopathy or other prion diseases (Zhao et al., 2018). Second, they more easily address religious- and consumer-related concerns than porcine-derived materials. Unavoidably, the present study still has some limitations. Swim bladders derived from different fish types probably have different properties; this deserves further investigation to determine the best fish resource. Furthermore, the structure and function of rabbit skin are quite different from those of human skin; large-animal experiments with skin closer to human skin structure are needed to further study the feasibility of the swim bladder material as a skin-repair material. Third, this experiment did not compare with the clinically-confirmed "gold standard" transplantation material, and the transplantation effect needs to be verified by further experimental comparison.

Conclusion

The introduction of swim bladders proposes a new method for healing large-scale skin defects caused by trauma and tumors. The decellularized swim bladders have good biocompatibility and can rapidly colonize wound sites to promote the growth of various surrounding cells, enabling the healing of skin defects. Excellent mechanical properties and increased thermal stability could be obtained after EDC/NHS crosslinking. The crosslinked swim bladders have the advantages of milder inflammatory reactions, more new blood vessels, higher healing efficiency, and smaller scars compared with un-crosslinked swim bladders in the whole process of healing. Furthermore, pores in both un-crosslinked and crosslinked swim bladders are suitable for cell adhesion and proliferation. This study confirms the safety and

effectiveness of swim bladders transplanted in animals, which can be a candidate for wound repair biomaterials.

Data availability statement

The original contributions presented in the study are included in the article/Supplementary Material; further inquiries can be directed to the corresponding author.

Ethics statement

The animal study was reviewed and approved by the Ethics Committee of Anhui Medical University.

Author contributions

LZ: investigation, original draft, and visualization. YL: formal analysis and data curation. WJ: conceptualization, review and editing, and project administration.

Conflict of interest

The authors declare that the research was conducted in the absence of any commercial or financial relationships that could be construed as a potential conflict of interest.

Publisher's note

All claims expressed in this article are solely those of the authors and do not necessarily represent those of their affiliated organizations, or those of the publisher, the editors, and the reviewers. Any product that may be evaluated in this article, or claim that may be made by its manufacturer, is not guaranteed or endorsed by the publisher.

Supplementary material

The Supplementary Material for this article can be found online at: https://www.frontiersin.org/articles/10.3389/fmats.2022.1037386/full#supplementary-material

References

Aghamirsalim, M., Mobaraki, M., Soltani, M., Kiani Shahvandi, M., Jabbarvand, M., Afzali, E., et al. (2022). 3D printed hydrogels for ocular wound healing. *Biomedicines* 10 (7), 1562. doi:10.3390/biomedicines10071562

Attasgah, R. B., Velasco-Rodríguez, B., Pardo, A., Fernández-Vega, J., Arellano-Galindo, L., Rosales-Rivera, L. C., et al. (2022). Development of functional hybrid scaffolds for wound healing applications. *iScience* 25 (4), 104019. doi:10.1016/j.isci.2022.104019

Behr, M., and Ganesan, K. (2022). Improving polysaccharide-based chitin/chitosan-aerogel materials by learning from genetics and molecular biology. *Mater. (Basel)* 15 (3), 1041. doi:10.3390/ma15031041

Birkelbach, M. A., Smeets, R., Fiedler, I., Kluwe, L., Wehner, M., Trebst, T., et al. (2020). *In vitro* feasibility analysis of a new sutureless wound-closure system based on a temperature-regulated laser and a transparent collagen membrane for laser tissue soldering (LTS). *Int. J. Mol. Sci.* 21 (19), 7104. doi:10.3390/ijms21197104

Chatterjee, S., Hui, P. C., Kan, C. W., and Wang, W. (2019). Dual-responsive (pH/temperature) Pluronic F-127 hydrogel drug delivery system for textile-based transdermal therapy. *Sci. Rep.* 9 (1), 11658. doi:10.1038/s41598-019-48254-6

Chen, P., Wang, A., Haynes, W., Landao-Bassonga, E., Lee, C., Ruan, R., et al. (2021). A bio-inductive collagen scaffold that supports human primary tendon-derived cell growth for rotator cuff repair. *J. Orthop. Transl.* 31, 91–101. doi:10.1016/j.jot.2021.10.006

Eun, J. B. C., Chung, H. J., and Hearnsberger, J. O. (1994). Chemical composition and microflora of channel catfish (*Ictalurus punctatus*) roe and swim bladder. *J. Agric. Food Chem.* 42 (3), 714–717. doi:10.1021/JF00039A022

Fernandes, R. M., Couto Neto, R. G., Paschoal, C. W., Rohling, J. H., and Bezerra, C. W. (2008). Collagen films from swim bladders: Preparation method and properties. *Colloids Surfaces B Biointerfaces* 62 (1), 17–21. doi:10.1016/j.colsurfb.2007.09.011

Fu, Y., Guan, J., Guo, S., Guo, F., Niu, X., Liu, Q., et al. (2014). Human urine-derived stem cells in combination with polycaprolactone/gelatin nanofibrous membranes enhance wound healing by promoting angiogenesis. *J. Transl. Med.* 12, 274. doi:10.1186/s12967-014-0274-2

Gaurav Kumar, P., Nidheesh, T., Govindaraju, K., Jyoti, S., and Suresh, P. V. (2017). Enzymatic extraction and characterisation of a thermostable collagen from swim bladder of rohu (Labeo rohita). *J. Sci. Food Agric.* 97 (5), 1451–1458. doi:10.1002/jsfa.7884

Gentile, P., and Garcovich, S. (2021). Systematic Review: Adipose-derived mesenchymal stem cells, platelet-rich plasma and biomaterials as new regenerative strategies in chronic skin wounds and soft tissue defects. *Int. J. Mol. Sci.* 22 (4), 1538. doi:10.3390/ijms22041538

Henderson, N. J., Fancourt, M., Gilkison, W., Kyle, S., and Mosquera, D. (2009). Skin grafts: A rural general surgical perspective. *ANZ J. Surg.* 79 (5), 362–366. doi:10.1111/j.1445-2197.2009.04890.x

Jafari, H., Lista, A., Siekapen, M. M., Ghaffari-Bohlouli, P., Nie, L., Alimoradi, H., et al. (2020). Fish collagen: Extraction, characterization, and applications for biomaterials engineering. *Polym. (Basel)* 12 (10), 2230. doi:10.3390/polym12102230

Jayakrishnan, A., and Jameela, S. R. (1996). Glutaraldehyde as a fixative in bioprostheses and drug delivery matrices. *Biomaterials* 17 (5), 471–484. doi:10.1016/0142-9612(96)82721-9

Kumar, V., Kumar, N., Gangwar, A. K., and Singh, H. (2015). Comparison of acellular small intestinal matrix (ASIM) and 1-ethyl-3-(3-dimethylaminopropyl) carbodiimide crosslinked ASIM (ASIM-EDC) for repair of full-thickness skin wounds in rabbits. *Wound Med.* 7, 24–33. doi:10.1016/j.wndm.2015.01.001

Łabuś, W., Kitala, D., Navarro, A., Klama-Baryła, A., Kraut, M., Sitkowska, A., et al. (2022). The urgent need to achieve an optimal strategic stock of human allogeneic skin graft materials in case of a mass disaster in Poland. *Cell Tissue Bank.*, 2022, 1–23. doi:10.1007/s10561-022-10001-z

Li, Q., Mu, L., Zhang, F., Sun, Y., Chen, Q., Xie, C., et al. (2017). A novel fish collagen scaffold as dural substitute. *Mater. Sci. Eng. C* 80, 346–351. doi:10.1016/j.msec.2017.05.102

Li, Y., Meng, H., Liu, Y., and Lee, B. P. (2015). Fibrin gel as an injectable biodegradable scaffold and cell carrier for tissue engineering. *Sci. World J.* 2015, 1–10. doi:10.1155/2015/685690

Litowczenko, J., Woźniak-Budych, M. J., Staszak, K., Wieszczycka, K., Jurga, S., and Tylkowski, B. (2021). Milestones and current achievements in development of multifunctional bioscaffolds for medical application. *Bioact. Mat.* 6 (8), 2412–2438. doi:10.1016/j.bioactmat.2021.01.007

Liu, Z., Xin, W., Ji, J., Xu, J., Zheng, L., Qu, X., et al. (2022). 3D-Printed hydrogels in orthopedics: Developments, limitations, and perspectives. *Front. Bioeng. Biotechnol.* 10, 845342. doi:10.3389/fbioe.2022.845342

Meng, Q., Sun, Y., Cong, H., Hu, H., and Xu, F. J. (2021). An overview of chitosan and its application in infectious diseases. *Drug Deliv. Transl. Res.* 11 (4), 1340–1351. doi:10.1007/s13346-021-00913-w

Mredha, M. T. I., Kitamura, N., Nonoyama, T., Wada, S., Goto, K., Zhang, X., et al. (2017). Anisotropic tough double network hydrogel from fish collagen and its spontaneous *in vivo* bonding to bone. *Biomaterials* 132, 85–95. doi:10.1016/j.biomaterials.2017.04.005

Mredha, M. T. I., Zhang, X., Nonoyama, T., Nakajima, T., Kurokawa, T., Takagi, Y., et al. (2015). Swim bladder collagen forms hydrogel with macroscopic superstructure by diffusion induced fast gelation. *J. Mat. Chem. B* 3 (39), 7658–7666. doi:10.1039/c5tb00877h

Parisi, M. G., Grimaldi, A., Baranzini, N., La Corte, C., Dara, M., Parrinello, D., et al. (2021). Mesoglea extracellular matrix reorganization during regenerative process in anemonia viridis (forskål, 1775). *Int. J. Mol. Sci.* 22 (11), 5971. doi:10.3390/ijms22115971

Pati, F., Datta, P., Adhikari, B., Dhara, S., Ghosh, K., and Das Mohapatra, P. K. (2012). Collagen scaffolds derived from fresh water fish origin and their biocompatibility. *J. Biomed. Mat. Res. A* 100 (4), 1068–1079. doi:10.1002/jbm.a.33280

Peng, X., Yue, P., Zhou, X., Li, L., Li, S., and Yu, X. (2019). Development and characterization of bladder acellular matrix cross-linked by dialdehyde carboxymethyl cellulose for bladder tissue engineering. *RSC Adv.* 9 (72), 42000–42009. doi:10.1039/c9ra07965c

Priyadarshani, P., Li, Y., Yang, S., and Yao, L. (2016). Injectable hydrogel provides growth-permissive environment for human nucleus pulposus cells. *J. Biomed. Mat. Res. A* 104 (2), 419–426. doi:10.1002/jbm.a.35580

Qiu, M., Chen, D., Shen, C., Shen, J., Zhao, H., and He, Y. (2016). Platelet-rich plasma-loaded poly(d, l-lactide)-Poly(ethylene glycol)-Poly(d, l-lactide) hydrogel dressing promotes full-thickness skin wound healing in a rodent model. *Int. J. Mol. Sci.* 17 (7), 1001. doi:10.3390/ijms17071001

Rittié, L. (2016). Cellular mechanisms of skin repair in humans and other mammals. *J. Cell Commun. Signal.* 10 (2), 103–120. doi:10.1007/s12079-016-0330-1

Saini, G., Segaran, N., Mayer, J. L., Saini, A., Albadawi, H., and Oklu, R. (2021). Applications of 3D bioprinting in tissue engineering and regenerative medicine. *J. Clin. Med.* 10 (21), 4966. doi:10.3390/jcm10214966

Shakya, P., Sharma, A. K., Kumar, N., Vellachi, R., Mathew, D. D., Dubey, P., et al. (2016). Bubaline cholecyst derived extracellular matrix for reconstruction of full thickness skin wounds in rats. *Sci. (Cairo)* 2016, 2638371–2638413. doi:10.1155/2016/2638371

Singh, H., Kumar, N., Sharma, A. K., Kataria, M., Munjal, A., Kumar, A., et al. (2014). Activity of MMP-9 after repair of abdominal wall defects with acellular and crosslinked bovine pericardium in rabbit. *Int. Wound J.* 11 (1), 5–13. doi:10.1111/j.1742-481X.2012.01031.x

Thongsuksaengcharoen, S., Samosorn, S., and Songsrirote, K. (2020). A facile synthesis of self-catalytic hydrogel films and their application as a wound dressing material coupled with natural active compounds. *ACS Omega* 5 (40), 25973–25983. doi:10.1021/acsomega.0c03414

Wang, S., Xiong, Y., Chen, J., Ghanem, A., Wang, Y., Yang, J., et al. (2019). Three dimensional printing bilayer membrane scaffold promotes wound healing. *Front. Bioeng. Biotechnol.* 7, 348. doi:10.3389/fbioe.2019.00348

Yang, F., Qin, X., Zhang, T., Lin, H., and Zhang, C. (2019). Evaluation of small molecular polypeptides from the mantle of pinctada martensii on promoting skin wound healing in mice. *Molecules* 24 (23), 4231. doi:10.3390/molecules24234231

Yoon, S. J., Hyun, H., Lee, D. W., and Yang, D. H. (2017). Visible light-cured glycol chitosan hydrogel containing a beta-cyclodextrin-curcumin inclusion complex improves wound healing *in vivo*. *Molecules* 22 (9), 1513. doi:10.3390/molecules22091513

You, D., Li, K., Guo, W., Zhao, G., and Fu, C. (2019). <p>Poly (lactic-co-glycolic acid)/graphene oxide composites combined with electrical stimulation in wound healing: Preparation and characterization</p>. *Int. J. Nanomedicine* 14, 7039–7052. doi:10.2147/IJN.S216365

Zhao, W. H., Chi, C. F., Zhao, Y. Q., and Wang, B. (2018). Preparation, physicochemical and antioxidant properties of acid- and pepsin-soluble collagens from the swim bladders of miiuy croaker (miichthys miiuy). *Mar. Drugs* 16 (5), 161. doi:10.3390/md16050161